SAND2011-2703C

Transient Stability and Performance Based on Nonlinear Power Flow Control Design of Renewable Energy Systems

David G. Wilson and Rush D. Robinett III
Sandia National Laboratories, Energy Technology & Systems Solutions Center,
P.O. Box 5800, Albuquerque, NM 87185

***Abstract*— In this paper, the swing equations for renewable generators are formulated as a natural Hamiltonian system with externally applied non-conservative forces. A two-step process referred to as Hamiltonian Surface Shaping and Power Flow Control (HSSPFC) is used to analyze and design feedback controllers for the renewable generator system. The results of this research include the determination of the required performance of a proposed Flexible AC Transmission System (FACTS)/storage device, such as a Unified Power Flow Controller (UPFC), to enable the maximum power output of a wind turbine while meeting the power system constraints on frequency and phase. The UPFC is required to operate as both a generator and load (energy storage) on the power system in this design. Necessary and sufficient conditions for stability of renewable generator systems are determined based on the concepts of Hamiltonian systems, power flow, exergy (the maximum work that can be extracted from an energy flow) rate, and entropy rate. An illustrative example demonstrates this HSSPFC methodology. It includes a 600 kW wind turbine, variable speed variable pitch configuration. The wind turbine is operated with a turbulent wind profile for below-rated wind power conditions. The wind turbine is connected in series through a UPFC to the infinite bus. Numerical simulation cases are reviewed that best demonstrate the stability and performance of HSSPFC as applied to a renewable energy system.**

I. Introduction

Wind energy is a variable generation source which should be considered as one part of a variable dynamically changing Electric Power Grid (EPG) infrastructure system. It is imparative that wind power be analyzed as an integral part of the EPG system. The size and flexibility of the power system are important aspects in assessing the overall system's capacity to accommodate large penetration of renewable energy sources such as wind power [1].

As wind turbines and other variable generation systems are influencing the behavior of the electric power grid by, interacting with conventional generation and loads, relevant models and details that can be integrated into power system simulations are needed. New modeling and control design methodologies which may include UPFC based on power electronics are being investigated [2], [3], [4], [5], [6] to help improve transient stability of renewable microgrids and inter-area power systems.

The goal of this paper is to present a step toward addressing the integration of renewable resources into the EPG by applying a new nonlinear power flow control technique [7], [8], [9] to the analysis of the swing equations for renewable generators connected to the EPG. Also, an initial investigation is preformed to maximize the energy capture from the wind turbine. This research extends the work initiated in references [10], [11], [12]. The results of this research include i) a HSSPFC design and comparision with conventional wind turbine controls in below-rated power conditions and ii) the determination of the required performance of a HSSPFC analysis of a FACTS/Storage device to enable the maximum power output of a wind turbine while meeting the power system constraints on frequency and phase. The FACTS/Storage device is required to operate as both a generator and load (energy storage) on the power system in this design.

This paper is divided into six sections. Section II presents the wind turbine model. Section III develops the adaptive HSSPFC controller for the wind turbine. Section IV develops HSSPFC for a OMIB and UPFC system with variable generation as an input. Section V discusses numerical simulations for i) the wind turbine control designs and ii) the UPFC control design that determines transient responses, power outputs, and energy requirements. Section VI summarizes the results with concluding remarks.

II. Wind Turbine Model

Typically, a variable-speed wind turbine aerodynamic power that is captured by the rotor is given [13], [14], [15] by

$$P_a = \frac{1}{2}\rho\pi R^2 C_P(\lambda,\beta)v^3$$

where ρ is the air density, R is the rotor radius, C_P is the power coefficient that depends on the tip-speed ratio, λ, and the blade pitch angle, β, and v is the wind speed. The tip-speed ratio is defined as

$$\lambda = \frac{\omega_r R}{v}$$

where ω_r is the rotor speed. The aerodynamic torque, T_a, can be identified from the power relationship

$$P_a = \omega_r T_a$$

where the aerodynamic torque expression becomes

$$T_a = \frac{1}{\rho}\pi R^3 C_T(\lambda,\beta)v^2$$

and the torque coefficient is related to the power coefficient by $C_T(\lambda,\beta) = C_P(\lambda,\beta)/\lambda$. The maximum theoretical

power that can be extracted by the wind is defined by the Betz curve. Betz determined that the maximum power that can be extracted by the wind turbine without losses is $C_{P_{max}}$ = 59%. For this study the C_P versus λ for the NREL CART machine [16] is shown in Fig. 1 with the corresponding characteristics given in Table I. This power curve includes the losses.

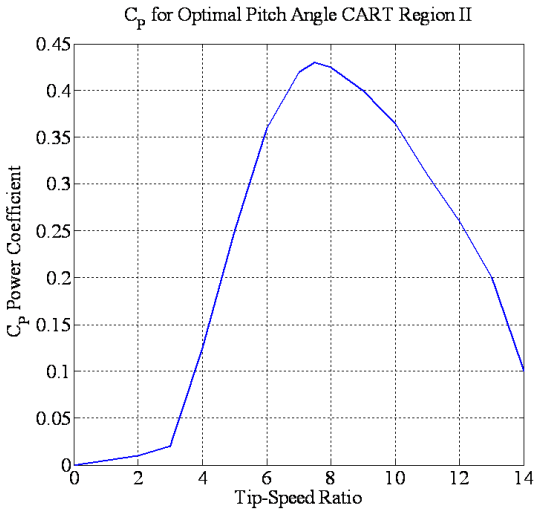

Fig. 1. Power curve for NREL CART wind turbine

TABLE I
CART WIND TURBINE CHARACTERISTICS

Rotor Diameter	43.3 m
Gearbox Ration	43.165
Hub height	36.6 m
Generator electric power	600 kW
Maximum rotor torque	162 kNm
Optimal tip-speed ratio	7.7

The power coefficient $C_P(\lambda, \beta)$ has a unique maximum that corresponds to the maximum power production. In addition, for below rated power, the blade pitch angle, $\beta = \beta_{opt}$ such that the optimal value $\lambda = \lambda_{opt}$ will be tracked thus

$$\omega_{r_{REF}} = \frac{\lambda_{opt}}{R} v.$$

In addition, the reference angular acceleration is defined as

$$\dot{\omega}_{r_{REF}} = \frac{\lambda_{opt}}{R} \dot{v}$$

where this development assumes that v and $\dot{v}$ are available and/or can be estimated. In this case a simple first-order estimator along with a derivative filter are used to generate these signals. The goal of the control system design is to maximize the wind power capture by adjusting the rotor speed ω_r to wind speed variation.

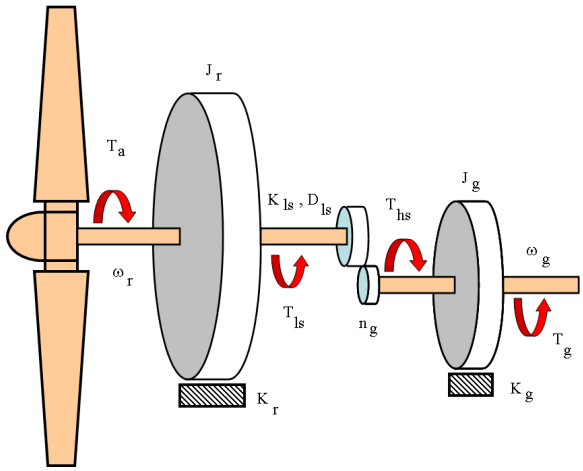

Fig. 2. Two mass wind turbine model

The wind turbine dynamics are given by the popular two-mass model (see Fig. 2) as

$$\begin{aligned} J_r\dot{\omega}_r &= T_a - T_{ls} - K_r\omega_r \\ J_g\dot{\omega}_g &= T_{hs} - K_g\omega_g - T_{em} \\ T_{ls} &= K_{ls}\left(\omega_r - \omega_{ls}\right) + D_{ls}\left(\theta_r - \theta_{ls}\right) \end{aligned}$$

where J_r is the rotor inertia, T_{ls} is the low-speed shaft torque, K_r is the rotor external damping, J_g is the generator inertia, T_{hs} is the high-speed shaft torque, K_g is the generator external damping, T_{em} is the electromagnetic torque, ω_{ls} is the low-speed rotational speed, θ_r is the rotor angle, θ_{ls} is the low-speed angle, and D_{ls} is the low-speed spring constant. The ideal gearbox ratio is defined as

$$n_g = \frac{T_{ls}}{T_{hs}} = \frac{\omega_g}{\omega_{ls}}.$$

For a very stiff rotor or assuming a perfectly rigid low-speed shaft, then a single-mass model for the wind turbine can be defined as

$$J_T\dot{\omega}_r = T_a - K_T\omega_r - T_g \tag{1}$$

where

$$\begin{aligned} J_T &= J_r + n_g^2 J_g \\ K_T &= K_r + n_g^2 K_g \\ T_g &= n_g T_{em}. \end{aligned}$$

This establishes the baseline wind turbine model used for the controller design.

III. ADAPTIVE POWER FLOW CONTROLLER DESIGN

The method known as the Indirect Speed Control (ISC) technique [15] is defined as

$$T_g = K_{opt}\omega_r^2 - K_T\omega_r$$

where K_{opt} is calculated based on tracking along the optimal aerodynamic efficiency C_P curve. For this study the ISC is considered the baseline controller that comparisons are made with the new adaptive power flow control design.

Following the nonlinear controller design methodology from reference [7], the Hamiltonian is defined as

$$\mathcal{H} = \frac{1}{2} J_T \left(\omega_r - \omega_{r_{REF}}\right)^2 + \frac{1}{2}\tilde{\Phi}^T \Gamma^{-1} \tilde{\Phi}. \tag{2}$$

From the wind turbine dynamic equation of motion Eq. (1) define

$$J_T \ddot{\theta}_r = M\dot{\theta}_r^2 - K_T \dot{\theta}_r - u$$

where $\ddot{\theta}_r = \dot{\omega}_r, M\dot{\theta}_r^2 = T_a, \dot{\theta}_r = \omega_r$, and $u = T_g$. Next define the control input as

$$u = u_{REF} + \Delta u$$

where

$$u_{REF} = M\dot{\theta}_r^2 - \hat{K}_T \dot{\theta}_r - \hat{J}_T \ddot{\theta}_{REF}$$

with $\hat{K}_T$ and $\hat{J}_T$ representing the estimate of the parameter and

$$\Delta u = K_D \left(\dot{\theta}_r - \dot{\theta}_{REF}\right)$$

where K_D is the derivative controller gain. The next step in the design is to take the derivative of the Hamiltonian Eq. (2) such that

$$\dot{\mathcal{H}} = \left[\left(\hat{J}_T - J_T\right)\ddot{\theta}_{REF} + \left(\hat{K}_T - K_T\right)\dot{\theta}_r - K_D\left(\dot{\theta}_r - \dot{\theta}_{REF}\right)\right]\left(\dot{\theta}_r - \dot{\theta}_{REF}\right) + \tilde{\Phi}^T \Gamma^{-1} \dot{\tilde{\Phi}} \tag{3}$$

then recognize and identify

$$\left(\hat{J}_T - J_T\right)\ddot{\theta}_{REF} + \left(\hat{K}_T - K_T\right)\dot{\theta}_r = Y\tilde{\Phi}$$

and substituting into Eq. (3) and simplifying yields

$$\dot{\mathcal{H}} = -K_D\left(\dot{\theta}_r - \dot{\theta}_{REF}\right) + \tilde{\Phi}^T\left[Y^T\left(\dot{\theta}_r - \dot{\theta}_{REF}\right) + \Gamma^{-1}\dot{\tilde{\Phi}}\right] \tag{4}$$

where

$$\begin{aligned} \tilde{\Phi}^T &= \left[\left(\hat{J}_T - J_T\right) \quad \left(\hat{K}_T - K_T\right)\right] \\ \dot{\tilde{\Phi}}^T = \dot{\Phi}^T &= \left[\dot{\hat{J}}_T \quad \dot{\hat{K}}_T\right] \\ Y &= \left[\ddot{\theta}_{REF} \quad \dot{\theta}_r\right]. \end{aligned}$$

Next set the last term in Eq. (4) to zero and solving for the adaptive parameter update equations yields

$$\begin{aligned} \dot{\hat{J}}_T &= -\gamma_1 \ddot{\theta}_{REF}\left(\dot{\theta}_r - \dot{\theta}_{REF}\right) \\ \dot{\hat{K}}_T &= -\gamma_2 \dot{\theta}_r\left(\dot{\theta}_r - \dot{\theta}_{REF}\right) \end{aligned}$$

where $\gamma_i, \ i = 1, 2$ are the positive definite adaptation controller gains. Assuming that the parameters cancel then a passivity design yields

$$\dot{\mathcal{H}} = -K_D\left(\dot{\theta}_r - \dot{\theta}_{REF}\right)^2.$$

Note that for a formal passivity design, the Hamiltonian Eq. (2) would be selected as the positive definite Lyapunov function.

IV. HSSPFC Applied to UPFC and Variable Generation

This section investigates power engineering models [6] that best reflect the new nonlinear power flow control methodology. Given

$$T_m - T_e = J\dot{\omega}_{RM} + B\omega_{RM} \tag{5}$$

$$\omega_{RM} = \frac{\omega}{N_p/2} \quad ; \quad \omega = \omega_{ref} + \dot{\delta} \tag{6}$$

and

$$T_m - T_e = \hat{J}\left(\dot{\omega}_{ref} + \ddot{\delta}\right) + \hat{B}\left(\omega_{ref} + \dot{\delta}\right) \tag{7}$$

then define the Hamiltonian as

$$\mathcal{H} = \frac{1}{2}\hat{J}\omega^2 \tag{8}$$

where the power flow or Hamiltonian rate becomes

$$\begin{aligned} \dot{\mathcal{H}} &= \hat{J}\dot{\omega}\omega \\ &= \left[T_m - T_e - \hat{B}(\omega_{ref} + \dot{\delta})\right]\left(\omega_{ref} + \dot{\delta}\right) \\ &= P_m - P_e - \hat{B}\omega^2. \end{aligned} \tag{9}$$

Next, add the approximate power flows from the generator, mechanical controls, and UPFC [6]

$$\begin{aligned} P_m &= P_{mc} + u_m(\omega_{ref} + \dot{\delta}) \\ P_e &= P_{ec}\sin\delta + u_{e1}P_{ec}\sin\delta - u_{e2}P_{ec}\cos\delta. \end{aligned} \tag{10}$$

Starting with the reference power flow equation

$$T_{m_{ref}} - T_{e_{ref}} = \hat{J}\dot{\omega}_{ref} + \hat{B}\omega_{ref} \tag{11}$$

with $\omega_{ref} = \textit{constant}$ and $\omega_{ref} >> \dot{\delta}$ and solving for the acceleration term gives

$$\hat{J}\ddot{\delta} = -\hat{B}\dot{\delta} + P_{m_e} + u_m\omega_{ref} - P_{e_c}\left[(1 + u_{e_1})\sin\delta - u_{e_2}\cos\delta\right].$$

Next define the Hamiltonian as

$$\mathcal{H} = \frac{1}{2}\hat{J}\dot{\delta}^2$$

then the derivative of the Hamiltonian becomes

$$\begin{aligned} \dot{\mathcal{H}} &= \hat{J}\ddot{\delta}\dot{\delta} \\ &= \Big[-\hat{B}\dot{\delta} + P_{m_c} + u_m\omega_{ref} - \\ &\quad P_{e_c}\left((1 + u_{e_1})\sin\delta - u_{e_2}\cos\delta\right)\Big]\dot{\delta}. \end{aligned}$$

Now assume that OMIB is combined with UPFC and $u_m = 0$ then

$$\hat{J}\ddot{\delta} + P_{e_c}\sin\delta - P_{m_c} = -\hat{B}\dot{\delta} - P_{e_c}\left[u_{e_1}\sin\delta - u_{e_2}\cos\delta\right]. \tag{12}$$

Next select the following nonlinear PID control laws from HSSPFC

$$\begin{aligned} u_{e_1} &= K_{P_e}\cos\delta_s + K_{D_e}\sin\delta\dot{\delta} + K_{I_e}\sin\delta\int_0^t \Delta d\tau \\ u_{e_2} &= K_{P_e}\sin\delta_s - K_{D_e}\cos\delta\dot{\delta} - K_{I_e}\cos\delta\int_0^t \Delta d\tau. \end{aligned} \tag{13}$$

where $\Delta = \delta - \delta_s$. Finally, substitute Eq. (13) into Eq. (12) yields the following

$$\hat{J}\ddot{\delta} + \left[P_{e_c}\sin\delta - P_{m_c}\right] + P_{e_c}K_{P_e}\sin(\delta - \delta_s)$$

$$= -\left[\hat{B} + P_{e_c} K_{D_e}\right] \dot{\delta} - K_{I_e} \int_0^t (\delta - \delta_s)\, d\tau.$$

The static stability condition becomes

$$\mathcal{H} = \frac{1}{2}\hat{J}\dot{\delta}^2 + P_{e_c}\left(1 + K_{P_e}\right)\left(1 - \cos(\delta - \delta_s)\right) \qquad (14)$$

with $\mathcal{H}$ being positive definite and

$$\delta_s = \sin^{-1}\left(P_{m_c}/P_{e_c}\right).$$

The dynamic stability condition for a passively stable control design yields

$$\oint_\tau \left[\hat{B} + P_{e_c} K_{D_e}\right] \dot{\delta}^2 dt > -\oint_\tau \left[P_{e_c} K_{I_e} \int_0^t (\delta - \delta_s) d\tau\right] \dot{\delta} dt. \qquad (15)$$

Clearly, the UPFC nonlinear PID controller expands the region of stability by increasing the PEBS from P_{e_c} to $P_{e_c}(1 + K_{P_e})$ and enabling the system to respond more quickly by adding an integrator to the dissipator of reference [6].

A feedforward control term can be added to the UPFC controllers, Eq. (13), for u_{e_1} and u_{e_2} and is defined by

$$\begin{aligned} u_{e_1} &= u_{e_1} - [(P_{m_{ref}} - P_m(t))/P_{max}] \sin\delta \\ u_{e_2} &= u_{e_2} + [(P_{m_{ref}} - P_m(t))/P_{max}] \cos\delta \end{aligned} \qquad (16)$$

where $P_{m_{ref}}$ is designed to emulate a constant input and $P_m(t)$ is from variable generation such as from wind or solar. In the next section these effects are explored further with the wind turbine model and adaptive HSSPFC control designed in the earlier section. The wind turbine control system electric power output is used to drive the $P_m(t)$ input variation to the OMIB combined with UPFC model which is representative of a below-rated power condition. The inertal constant for the OMIB defined by [6] has been modified (reduced) to reflect the same inertial parameters (see Appendix) for a 600kW wind turbine generator system. This approach expands on [12] by including the actual power output of the wind turbine.

V. Numerical Simulations

A numerical example (based on an example in [6] all parameters are given in the Appendix) for a OMIB with a UPFC controller is used to demonstrate the controllers defined in earlier sections. In addition, simple wind turbine generator characteristics are investigated by allowing the P_m term to become time-varying in the swing equations. The OMIB system is shown schematically in Fig. 3.

A. Wind Turbine Control Simulation

As a numerical example, an 7 mps turbulent wind condition [17] was used as the driving wind input as shown in Fig. 4. Both controller designs were run and comparisons were made. In Figure 5 the rotor speed responses are shown. The optimal rotor speed is shown in green, ω_{opt}, the estimated rotor speed in black, ω_{est}, the power flow control rotor speed is shown in blue, ω_{PFC}, and the baseline ISC rotor speed is shown in red, ω_{base}. From the responses the power flow controller tracks the estimate rotor speed

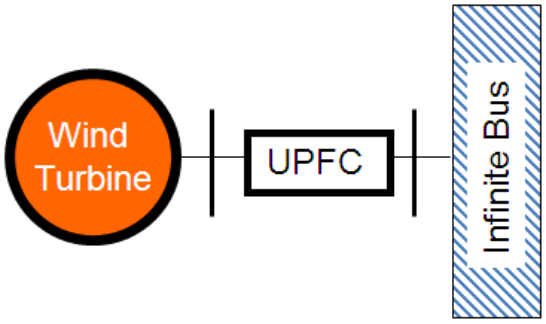

Fig. 3. One machine infinite bus model with UPFC and wind turbine generator

more closely then the baseline controller. Hence, in Figure 6, where the electrical power generated is shown, the power flow control generates on the average 28.5% more power than the baseline control. Note that this still requires a detailed wind simulator investigation and verification of acceptable wind turbine loading conditons. However, the initial results look promising.

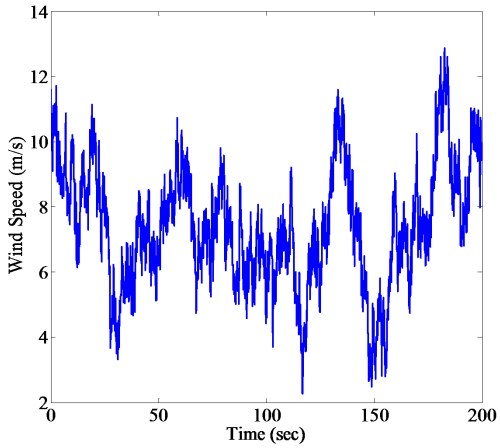

Fig. 4. Turbulent wind condition IEC NTM Type A 7 mps

B. UPFC Control Simulation

Initially, the OMIB with UPFC is given a faulted initial condition that is away from the stable equilibrium point. The control system gains K_{P_e}, K_{D_e}, and K_{I_e} are designed to ensure static stability and dynamic stability conditions and were adjusted for tolerable transient responses. The feedfoward portion help to produce a flat power response, such that the UPFC performs as an OMIB system. The electrical power output from the adaptive HSSPFC wind turbine design was employed in series to drive the OMIB with UPFC system as an input through $P_m(t)$.

In these simulation results δ_1 represents feedback only and δ_2 represents, both feedback and feedforward, respectively. The phase plane and transient responses for both δ_1 and δ_2 are given in Figs. 7 and 8, respectively. Figure 9 presents the transient power flow responses. The wind input is given

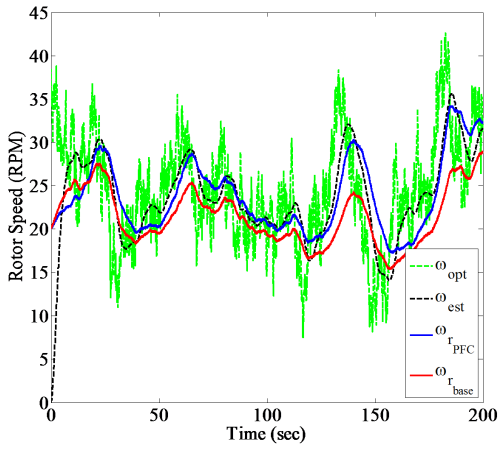

Fig. 5. Transient responses for rotor speed

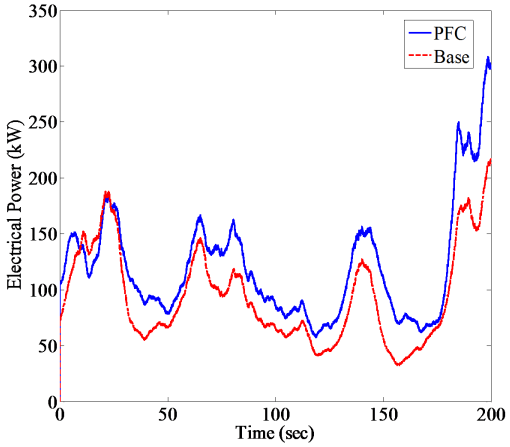

Fig. 6. Transient responses for generated electric power

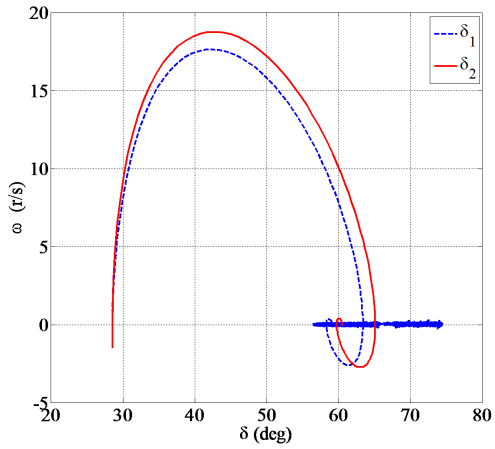

Fig. 7. Phase plane for OMIB with UPFC δ_1 response is with UPFC feedback PID control only and δ_2 response is for adding feedforward control in addition to feedback control

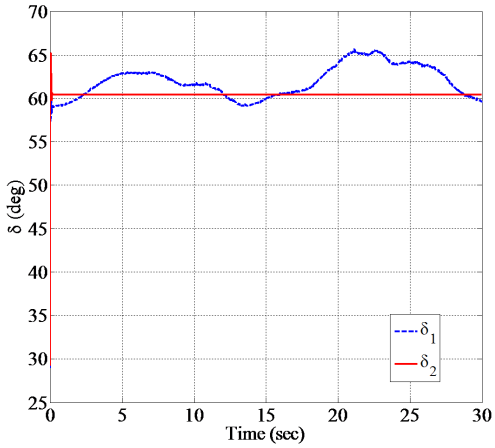

Fig. 8. Transient machine angle responses for OMIB with UPFC PID feedback control only δ_1 response and δ_2 response is for adding feedforward control

as the green trace and the responses for both δ_1 and δ_2 are shown as the blue and red traces, respectively. The difference between the varying wind power input and the UPFC output are defined as $P_{ref_i} = P_{wind} - P_{UPFC_i}, i = 1, 2$. The corresponding energy storage transient responses for each of the UPFC systems are given in Fig. 10. These results help to define the power and energy storage requirements for the wind turbine OMIB with UPFC system.

VI. Summary and Conclusions

The swing equations for renewable generators connected to the grid were developed and a wind turbine model and advanced controller was used as a variable generation example. A nonlinear control design example was employed to demonstrate the HSSPFC technique for the OMIB system with a UPFC and wind turbine. The system characteristics were explored to determine the needed performance of the UPFC to enable the maximum power output of a wind turbine while meeting the power system constraints on frequency and phase. The nonlinear PID feedback controller design along with feedfoward control for the OMIB system with a UPFC was shown to be an extension of the Control Lyapunov Function approach. Numerical simulations of the wind turbine system design were reviewed. The results demonstrated the requirements of the UPFC systems as well as the value of the feedforward control. In the near future, HSSPFC will be applied to multiple machines including gas turbine generators combined with wind turbines and FACTS devices.

Acknowledgments

Sandia National Laboratories is a multiprogram laboratory operated by Sandia Corporation, a Lockheed Martin Company, for the U.S. Department of Energy's National Nuclear Security Administration under contract DE-AC04-94AL85000.The first author is a member of the technical staff, dwilso@sandia.gov and the second author is a senior

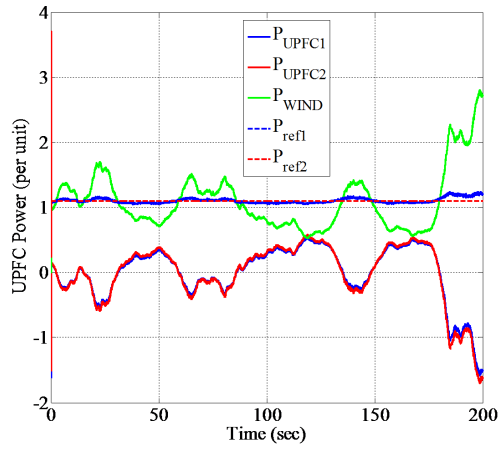

Fig. 9. Transient power flow responses for OMIB with UPFC δ_1, δ_2, wind input, and references (difference between UPFC and wind power input) , respectively

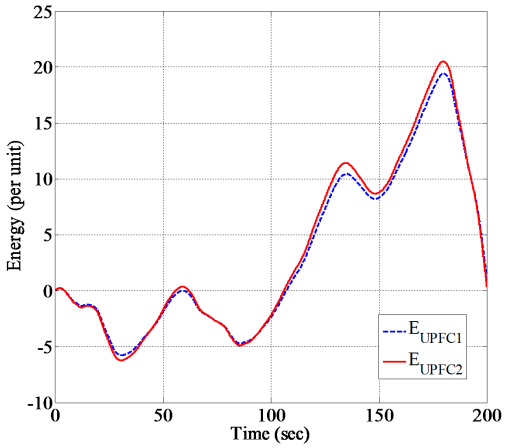

Fig. 10. Transient energy responsed for OMIB with UPFC δ_1 and δ_2, respectively

manager, rdrobin@sandia.gov, at Sandia National Laboratories, respectively.

REFERENCES

[1] F. Van Hulle and P. Gardner, *Wind Energy - The Facts: PART II Grid Integration*, EWEA and Garrad Hassan, 2007.

[2] E.S. Abdin and W. Xu, *Control Design and Dynamic Performance Analysis of a Wind Turbine-Induction Generator Unit,* IEEE Trans. on Energy Conversion, Vol. 15, No. 1, March 2000.

[3] J.G. Slootweg, S.W.H. de Haan, H. Polinder, and W.L. Kling, *General Model for Representing Variable Speed Wind Turbines in Power System Dynamic Simulations*, IEEE Trans. on Power Systems, Vol. 18, No. 1, Feb. 2003.

[4] W.-L. Chen and Y.-Y. Hsu, *Controller Design for an Induction Generator Driven by a Variable-Speed Wind Turbine*, IEEE Trans. on Energy Conversion, Vol. 21, No. 3, Sept. 2006.

[5] P. Kumkratug, *Application of UPFC to Increase Transient Stability of Inter-Area Power Systems*, Journal of Computers, Vol. 4, No. 4, April 2009.

[6] M. Ghandhari, *Control Lyapunov Functions: A Control Strategy for Damping of Power Oscillations in Large Power Systems*, Doctoral Dissertation, TRITA-EES-0004, ISSN 1100-1607, Royal Institute of Technology, Stockholm, Sweden, 2000.

[7] R..D. Robinet III and D.G. Wilson, "Exergy and Irreversible Entropy Production Thermodynamic Concepts for Control System Design," *International Journal of Exergy,* Vol. 6, No. 3, 2009, pp. 357–387.

[8] R.D. Robinet III and D.G. Wilson, "What is a Limit Cycle?," *International Journal of Control,* Vol. 81, No. 12, December 2008, pp. 1886–1900.

[9] R.D. Robinett III and D.G. Wilson, "Exergy and Entropy Thermodynamic Concepts for Control System Design: Slewing Single Axis," *AIAA Guidance, Navigation, and Control Conference and Exhibit,* Keystone, CO., August 2006.

[10] R.D.Robinett III and D.G. Wilson, *Transient Stability and Control of Renewable Generators Based on Hamiltonian Surface Shaping and Power Flow Control: Part I - Theory*, invited paper, 2010 IEEE Multi-Conference on Systems and Control, Sept. 8-10, 2010, Yokohama, a port city on Tokyo Bay, Japan.

[11] D.G. Wilson and R.D. Robinett III, *Nonlinear Power Flow Control Applications to Conventional Generator Swing Equations Subject to Variable Generation*, International Symposium on Power Electronics, Electrical Drives, Automation and Motion, SPEEDAM 2010, June 14-16, Pisa, Italy.

[12] D.G. Wilson and R.D. Robinett III, *Transient Stability and Control of Wind Turbine Generation Based on Hamiltonian Surface Shaping and Power Flow Control*, 9th International Workshop on Large-Scale Integration of Wind Power into Power Systems as well as on Transmission Networks for Offshore Wind Power Plants, October 2010, Quebec City, Quebec, Canada.

[13] B. Boukhezzar, H. Siguerdidjane, and M. Hand, *Nonlinear Control of Variable Speed Wind Turbines for Load Reduction and Power Optimization*, 44th AIAA Aerospace Science Meeting and Exhibit, Jan. 2006, Reno, Nevada.

[14] Song, Y.D., Dhinakaran, B., and Bao, X.Y., *Variable Speed Control of Wind Turbines using Nonlinear and Adaptive Algorithms*, Journal of Wind Engineering and Industrial Aerodynamics, 85 (20000) pp. 293-308.

[15] W.E. Leithead and D. Connor, *Control of Variable Speed Wind Turbines: Design Task*, International Journal of Control, Vol. 73, 2000, pp. 1173-1188.

[16] A.D. Wright, *Modern Control Design for Flexible Wind Turbines*, NREL Technical Report, NREL/TP-500-35816, July 2004.

[17] NWTC Design Codes (AirfoilPrep by Dr. Craig Hansen). http://wind.nrel.gov/designcodes/preprocessors/airfoilprep/. Last modified 16-January-2007; accessed 16-January-2007.

APPENDIX

The numerical values for existing OMIB system example from [6] with modifications noted:

$$
\begin{aligned}
\hat{J}' &= \frac{2H}{\omega_o} = \frac{2(0.2268)}{100\pi} \quad \textit{H based on 600kW turbine} \\
\hat{B}' &= \frac{2}{\omega_o} \\
P_m &= 1.1(p.u) \\
P_{max} &= bE'V = 1.2647 \\
b &= \frac{1}{x_L} = \frac{1}{0.85} \\
E' &= 1.075(p.u) \\
V &= 1.0(p.u)
\end{aligned}
$$

where $\hat{J}'$ and $\hat{B}'$ are scaled by $\omega_o = 50Hz \cdot (2\pi)$ rad/sec.